Published in "Food Chemistry 133(4): 1435–1440, 2012"
which should be cited to refer to this work.

Enhanced electrochemical performance of <30 nm thin $LiMnPO_4$ nanorods with a reduced amount of carbon as a cathode for lithium ion batteries

Nam Hee Kwon*, Katharina M. Fromm

Department of Chemistry, University of Fribourg, Chemin du Musée 9, CH-1700 Fribourg, Switzerland

5–10 nm thin rod shaped $LiMnPO_4$ nanoparticles are synthesized by an improved thermal decomposition method. The synthesis parameters such as the concentration of surfactants, reaction temperature and time, as well as the presence of a solvent play a critical role in the formation of spherical, thin or thick nanorods, and needle-shaped particles of $LiMnPO_4$. A washing procedure to efficiently eliminate the surfactants attached to the surface of $LiMnPO_4$ nanoparticles is presented, avoiding thermal treatment at high temperatures. A nanocomposite $LiMnPO_4$ electrode provides a discharge capacity of 165 mAh/g at 1/40 C and 66 mAh/g at 1 C with only 10 wt% of total carbon additive. The characteristics of as-synthesized and low amount of carbon coated $LiMnPO_4$ are described as well as their electrochemical properties.

1. Introduction

Commercial lithium ion batteries are cobalt-based and limited to applications in small portable electronic devices due to the practical capacity limitation [1–3], cost and safety issues [4,5]. Future energy storage devices need advanced materials to fulfill the higher demands in terms of energy density and safety, while reducing the cost and environmental concerns. Olivine $LiMPO_4$ (M = Fe, Mn, Co and Ni) materials recently gained interest as alternative cathode material because of their thermal/chemical stability and low cost [6]. Contrary to metal oxide materials such as $LiCoO_2$, $LiMn_2O_4$, $LiNiO_2$, $LiMnO_2$, etc., olivines have PO_4^{3-} polyanions, which make the structure stable vs. lithium insertion/extraction [6,7]. Among the olivine materials, $LiFePO_4$ was firstly developed and is available on the market. However, its energy density related with the low cell voltage (3.4 V vs. Li) and the theoretical capacity (170 mAh/g) limits its use in electric vehicles [7]. $LiMnPO_4$ has also 170 mAh/g of theoretical capacity but has a higher cell voltage of 4.1 V vs. Li, thus providing a higher energy density than $LiFePO_4$ [8,9]. In order to allow the $Mn^{2+/3+}$ redox reaction in a $LiMnPO_4$ cathode, the material needs to be both ionically and electronically conductive for Li^+ diffusion and electron transport, respectively. However, pure $LiMnPO_4$ material suffers from poor intrinsic electronic conductivity [10,11]. To improve the electrochemical kinetics, several groups, including previous work by us, reported the enhanced electrochemical properties, combining both, reduced particle size of $LiMnPO_4$ and carbon coating [12–15]. Nanosized $LiMnPO_4$ provides the shorter lithium ion diffusion path within a single particle compared to micronsized $LiMnPO_4$ [16]. Most highly performing $LiMnPO_4$ materials were achieved by adding a large amount of carbon (15–30 wt%) in order to increase the electronic conductivity [12–15,17–20].

Nano-$LiMnPO_4$ has been prepared by various wet chemical methods such as hydrothermal [21–23], thermal decomposition [20,24], solvothermal [17,25], polyol methods [15], etc. Wet chemical methods are preferable as they allow perfect mixing of precursors, better homogeneity and more regular morphology to obtain nanosized particles. However, a drawback of this method is the complete removal of organic residuals, which prohibit the conductivity of the so synthesized material. Doi et al. obtained $LiMnPO_4$ having uniform particle sizes of 7 nm via the thermal decomposition method. Its initial discharge capacity was only about 6 mAh/g even though the charge and discharge rates were extremely slow (1/100 C) [24]. The poor electrochemical performance of $LiMnPO_4$ even with 7 nm sized particles is explained by the presence of remaining oleic acid on $LiMnPO_4$ particles after the synthesis, preventing Li^+ and electron transfer. While the thermal treatment allows to burn out the attached oleic acid on $LiMnPO_4$, this process results in 40–125 nm thick rod shaped $LiMnPO_4$ instead of 7 nm spherical shape of particles, providing 65 mAh/g of capacity at 1/100 C with an additive of 25 wt% of carbon. Thus, to make ultrafine nano-$LiMnPO_4$ particles electrochemically active, the clean surface of nano-$LiMnPO_4$ particles without thermal treatment is necessary.

* Corresponding author. Tel.: +41 26 300 87 35; fax: +41 26 300 97 38.
E-mail addresses: namhee.kwon@unifr.ch (N.H. Kwon), katharina.fromm@unifr.ch (K.M. Fromm).

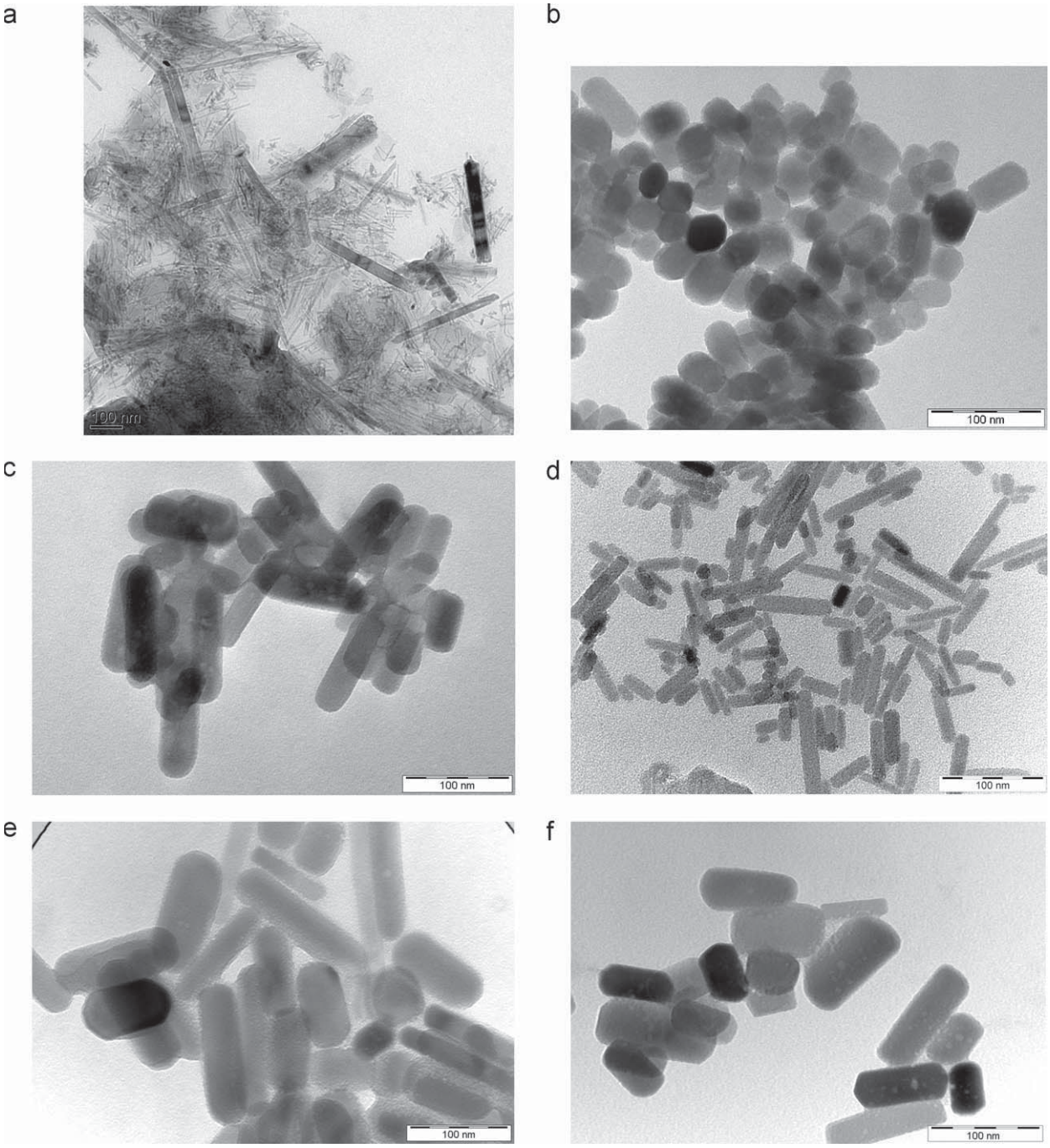

Fig. 1. TEM images show various shapes and sizes of $LiMnPO_4$ nanoparticles synthesized via thermal decomposition method. The syntheses parameters are following: (a) using only a surfactant at a molar ratio 9:1 of oleic acid and precursors at 280 °C for 1 h. (b)–(f) using both a surfactant and benzyl ether at a molar ratio 9:1 of oleic acid and precursors at 265 °C for 1 h (b) and 4 hrs (c), at a molar ratio 3:1 at 265 °C for 1 h (d), 280 °C for 1.5 h (e) and 280 °C for 1 h (f).

The carbon coating must be permeable for Li^+ ions in the electrolyte to be penetrated into the active material. Nanostructured composites consisting of the cathode material and a conductive additive allow to utilize theoretical capacity [13,14,26]. There are several parameters to be taken into account in order to make a nanocomposite applicable as a cathode material for lithium ion batteries. Increasing the amount of carbon in the electrode enhances its electronic conductivity [12], but as carbon is not electrochemically active, minimizing the amount of carbon is desired for increasing the loading of active material within a given volume of lithium ion batteries in order to increase the energy density. This is particularly important for large applications such as electric vehicles where high power and energy density are required. In addition, the nanostructure of the composite can be dependent on the morphology and surface area of the carbon additive as well as its preparation method. For example, porous carbon black is spherical and has high surface area, [27–29] while graphite is a sheet structure and has relatively low surface area [28]. Thus, nanocomposites of $LiMnPO_4$ with 20% or more high surface area carbon black were shown to provide large contact area with the active material, leading to homogeneous nanostructured composites [13,15].

So far, the production of electrochemically active and surfactant-free nanoparticulate $LiMnPO_4$ <30 nm remains a challenge, together with the reduction of carbon amount while

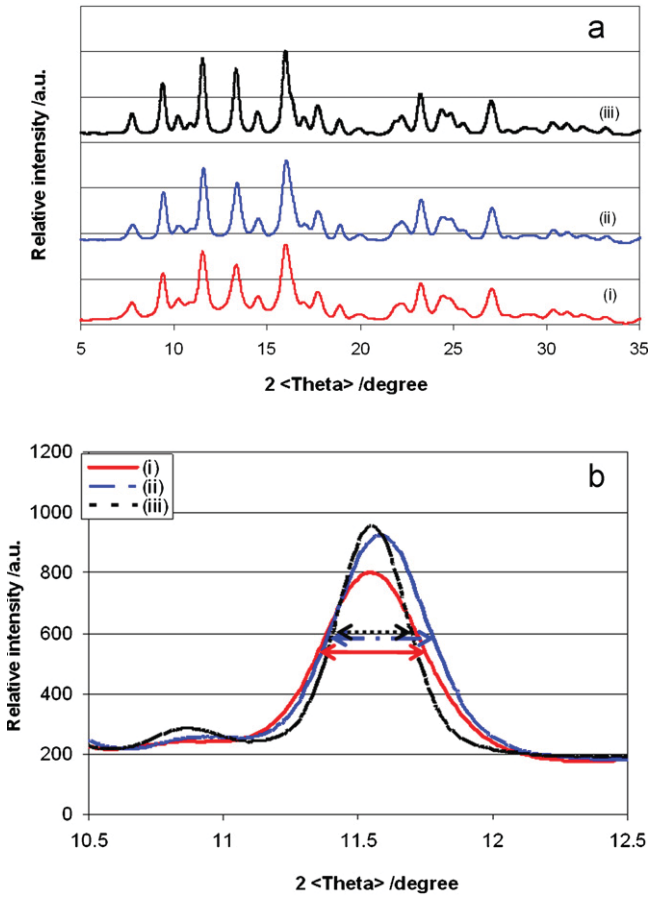

Fig. 2. (a) Full XRD patterns of $LiMnPO_4$ prepared by different synthesis conditions. (b) A full width at a half maximum (FWHM) of various crystal sizes of $LiMnPO_4$ materials. (i) Phase N, (ii) Phase NR and (iii) Phase TR of $LiMnPO_4$.

maintaining high performance of nanocomposite C-$LiMnPO_4$ electrode. In this study, we address the questions how to reduce efficiently the $LiMnPO_4$ particle size and the influence of the reaction conditions on the shape of the nanoparticles, how to eliminate organic residues on the surface of the latter, and how to reduce the amount of added carbon for the production of the electrode, while still maintaining excellent electrochemical properties.

2. Experimental

$LiMnPO_4$ material is prepared by the thermal decomposition method [24] without or with high boiling temperature solvent of benzyl ether. 3 mmol $Mn(NO_3)_2{\cdot}6H_2O$ and 3 mmol $LiOH{\cdot}H_2O$ are dissolved in 9 or 27 mmol oleic acid at 120 °C. In case of using a solvent, 20 ml of benzyl ether was then added to the solution. When the temperature of the solution reaches 230 °C, 9 or 27 mmol oleylamine and 3 mmol H_3PO_4 are injected. The solution is kept stirring vigorously and is held at 230 °C for 1.5 h. Then the temperature is increased to between 265 and 280 °C for 1–4 h. After the reaction, the suspension was centrifuged to collect the sedimented black powder. This material is rinsed with ethanol and hexane and centrifuged.

In order to remove the organic residue after rinsing, the collected black material was dispersed in 15 ml chloroform in a glass tube. Deionized water containing 0.1 g of citric acid is added to the tube, forming a two-phase system. The black chloroform solution clearly separates from the water phase in the tube. The mixture is stirred while heating overnight at 85 °C. The transparent water became a gray suspension after ligand exchange. This gray suspension was centrifuged to collect the gray powder.

As-synthesized $LiMnPO_4$ after ligand exchange was mixed with 5 or 7 wt% of carbon black using a ball mill (RETSCH) for 10–90 min.

As-synthesized $LiMnPO_4$ material and C-$LiMnPO_4$ composite have been characterized by various methods. X-ray diffraction using Mo-radiation (give machines here and below) was employed to identify the phase. Brunauer–Emmett–Teller (BET) nitrogen absorption method was applied to measure the specific surface area. Thermogravimetric analysis (TGA) was used for thermal analysis. The morphology and the size of particles were determined by scanning electron microscopy (SEM, Philips XL30), transmission electron microscopy (TEM) and high-resolution transmission electron microscopy (HRTEM). Fourier transform infrared (FT-IR) was employed for the surface analysis. The crystallite size is calculated by the Scherrer equation ($d = 0.9\lambda/(B\cos\theta)$), where d is the mean crystallite size in volume–weight, λ is the wavelength of the X-rays, B is the width of a peak at a half maximum due to size effects assuming that there is no strain, K is a constant value of 0.89, and θ is the Bragg angle).

For the electrochemical property, the electrode was prepared on aluminium foil with C-$LiMnPO_4$ composite, carbon black and polyvinylidene fluoride (PVDF) in N-methyl-2-pyrrolidone (NMP). The weight ratio of active material $LiMnPO_4$, carbon black and the binder was 80:10:10. After drying the electrode at 120 °C under vacuum overnight, the working electrode was assembled with lithium metal as counter electrode, ethyl carbonate (EC) and dimethyl carbonate (DMC) mixture in 1:1 volume ratio with 1 M $LiPF_6$ electrolyte and a separator from Celgard in Swagelok cell. Potentiostat and Galvanostat technique were applied to obtain the electrochemical property of C-$LiMnPO_4$ composite electrodes using Arbin 2000 instrument.

3. Results and discussion

3.1. Synthesis of $LiMnPO_4$ nanoparticles

In a first step we tried to reproduce the spherical $LiMnPO_4$ particles of 7 nm obtained by Doi et al., repeating their synthetic procedure [24]. However, under the described conditions, we could not reproduce their results, obtaining nanorods of 5 nm with very low yield (<30%) shown in Fig. 1(a) (hereafter referring to as phase N for needle). In order to improve the yield, we used benzyl ether as solvent because it has a high boiling point and is a good solvent for all used precursors ($LiOH{\cdot}H_2O$, $Mn(NO_3)_2{\cdot}6H_2O$, and H_3PO_4) during the synthesis. The yield of $LiMnPO_4$, identified by XRPD, could be improved to over 78%. In the following, we investigated the shape and size of $LiMnPO_4$ nanoparticles obtained as a function of reaction temperature, reaction time and the relative amounts of the surfactants.

The influence of the concentration of surfactant and reaction time on the thickness on size and shape of $LiMnPO_4$ is shown in Fig. 1(b)–(d). A molar ratio of 9:1 of oleic acid and precursor with the reaction temperature of 265 °C for 1 h provides spherical, slightly elongated shapes of particles of 30–50 nm shown Fig. 1(b) (hereafter referring to as phase S for spherical). After 4 h of reaction time and otherwise same conditions, we obtained rod-shaped $LiMnPO_4$ of 30 nm × 100 nm (Fig. 1(c)). Lowering the concentration of the surfactant to a molar ratio 3:1 of oleic acid to precursors, we obtain rod-shaped particles, which are thinner (10–20 nm) than the ones obtained before (Fig. 1(d) hereafter referring to as phase NR for nanorods).

The temperature during the synthesis also influences the thickness of nanorod shapes, as shown in Fig. 1(d)–(f). For a reaction time of 1.5 h, a high temperature of 280 °C gives 50 nm thick nanorods

Table 1
A summary of the crystallite size and specific surface area of $LiMnPO_4$ materials with various shapes of nanoparticles.

Shape of particles	Size of crystallite (nm)	S_{BET} (m^2/g)	Particle size by S_{BET} [a] (nm)	Size by TEM (nm)
Needle and rod	16	80.35	22	$5 \times (30–100)$ $(30–50) \times (200–300)$
Thin rod	18	98.78	18	$(10–20) \times (30–100)$
Sphere	21	35.07	49	30–50
Thick rod	24	18.24	95	$(15–50) \times (62–165)$

[a] The particle size, d is calculated by the equation of $d = K/(\rho\, S_{BET})$, where K is the shape factor, ρ is the density of the material and S_{BET} is the specific surface area of the material.

(Fig. 1(e)) compared to 10 nm at 265 °C (Fig. 1(d)). Reducing the reaction time to 1 h at 280 °C leads to shorter rodlike particles with (15–50) nm × (62–165) nm (Fig. 1(f)) (hereafter referring to as phase TR for thick nanorods).

For the synthesis aspects, we can conclude that the smallest particles are still obtained without solvent but with very low yield, while we obtain excellent yields of as small as 10 nm sized $LiMnPO_4$ particles in presence of a solvent. The external parameters like the concentration of surfactant, the reaction temperature and the duration of the synthesis play an important role to control the shape and size of nanoparticles. The best conditions in our studies are the ratio of 3:1 of oleic acid to precursors, the reaction temperature 265 °C and the time of 1.5 h, leading to 10 nm × 30 nm of $LiMnPO_4$ particles.

The crude material obtained from all these syntheses was found to have organic material on the surface, which we were able to remove with special washing procedure described in Section 3.3. Fig. 1 refers to the particles obtained after the washing process.

3.2. Crystallite size and specific surface area of $LiMnPO_4$

We determined the crystallite size using Scherrer equation applied to X-ray powder diffractograms (Fig. 2(a)) of our $LiMnPO_4$ nanoparticles obtained under the different conditions. We chose the XRD peak at $2\theta = 11.6°$ as it has high enough intensity and no shoulder from neighbouring peaks. From the different peak widths of three samples corresponding to phase N, NR and TR in Fig. 1(a),

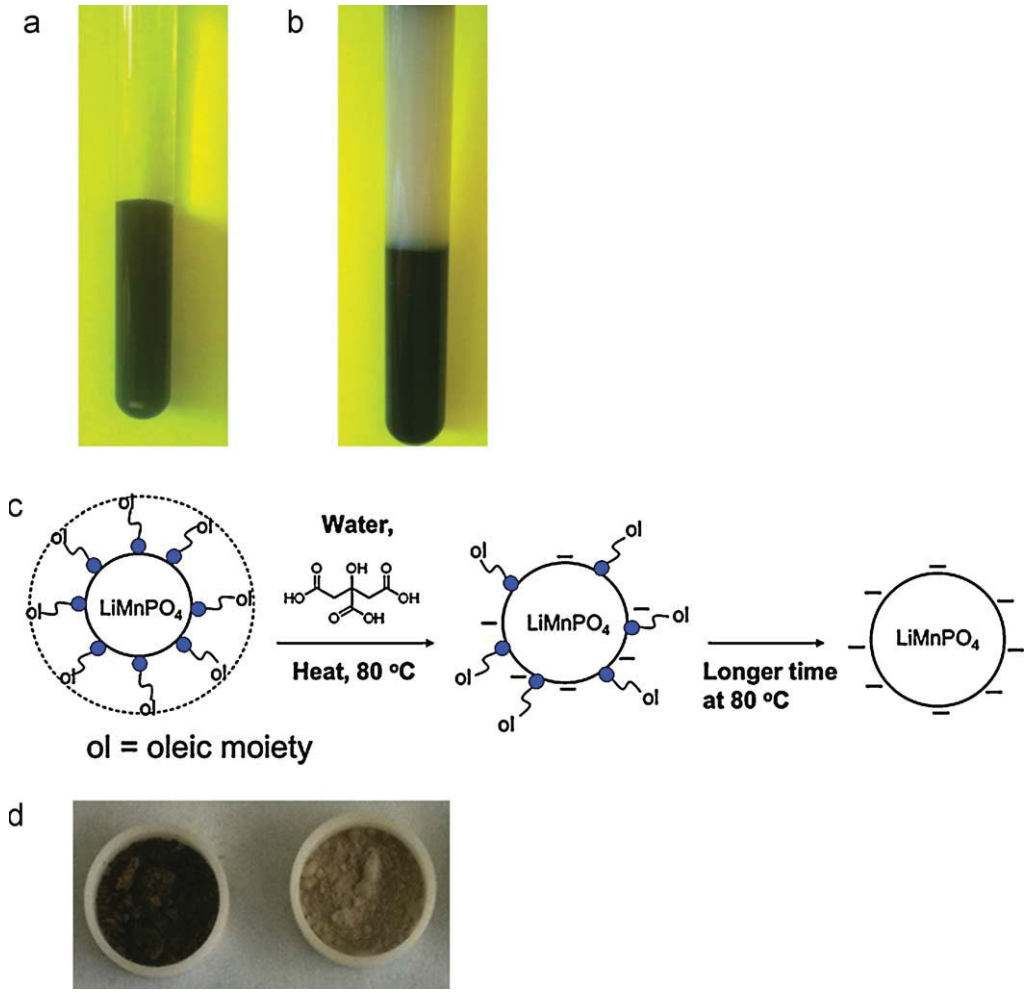

Fig. 3. (a) Before ligand exchange; (b) after ligand exchange; (c) a scheme of the process of $LiMnPO_4$ surface modification; (d) the dark brown $LiMnPO_4$ material coated with oleic acid and oleylamine (on the left) and light gray one without oleic acid (on the right). (For interpretation of the references to color in this figure legend, the reader is referred to the web version of the article.)

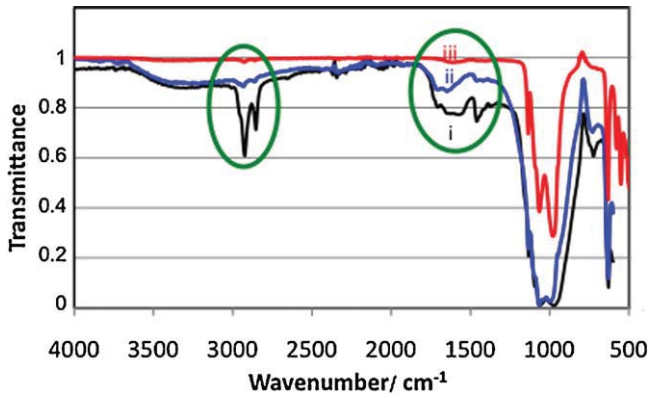

Fig. 4. FT-IR of various $LiMnPO_4$ samples: (i) coated with surfactant (before washing), (ii) washed with ethanol/hexane and (iii) ligand exchanged with citric acid aqueous solution.

(d) and (f), respectively, we can conclude that the crystallite sizes vary between 16 and 24 nm on average.

The specific surface areas (SSA) of various shaped and sized $LiMnPO_4$ are analyzed using N_2 adsorption method. The characteristics of various as-synthesized $LiMnPO_4$ nanoparticles are summarized in Table 1. The thin nanorod shaped $LiMnPO_4$ corresponding to Fig. 1(d) obtained the highest SSA of ca.100 m^2/g corresponding to 18 nm of particle size assuming spherical particle. The needle shaped nanoparticles have slightly lower SSA, 80 m^2/g, due to the small amount of large rod shaped $LiMnPO_4$ particles observed in Fig. 1(a). The sphere and thin rod shaped $LiMnPO_4$ particles corresponding to phase S and phase NR, have specific surface areas of ~35 and 99 m^2/g, respectively. The characteristics of four samples, phase N, NR, S and TR are summarized in Table 1.

3.3. Washing procedure of $LiMnPO_4$ nanoparticles

After the synthesis of $LiMnPO_4$ nanoparticles, the material is described to be rinsed with ethanol and hexane in order to remove the surfactants attached on the surface of $LiMnPO_4$ [24]. However, the surfactants were not completely eliminated, as indicated by the dark brown color of the product. We observed that for the synthesis in which we use the solvent, the surfactant can be removed better compared to syntheses without solvent – but not totally. As we do not want risk the increase of the particle size by thermal treatment for the removal of organic residues, we tested another 'washing' method called "ligand exchange" [30–32]. For this ligand exchange, we start by collecting the material first by using centrifugation after the synthesis. It is then dispersed in $CHCl_3$. A solution of citric acid in water is added, yielding a two-phase system. (Fig. 3(a)) Mild heating at 80 °C leads to the formation of boiling $CHCl_3$, forming droplets, which move up through aqueous solution before evaporating. These small droplets are in close contact with the aqueous phase, and the exchange of oleic acid and oleylamine vs. citric acid can occur at the surface of $LiMnPO_4$ nanoparticles in suspension in these droplets. Citrate decorated $LiMnPO_4$ nanoparticles are preferably suspended in water rather than $CHCl_3$, and therefore we observe the phase transfer of the nanoparticles from the organic into the aqueous phase (Fig. 3(b)). The rinsing process is shown in Fig. 3(c). The ligand exchange is accompanied by a color change from dark brown to light gray (Fig. 3(d)). The gray material is confirmed to be $LiMnPO_4$ by XRPD after ligand exchange and centrifugation (see Supplementary data Fig. S1).

The ligand exchange process on the surface of $LiMnPO_4$ nanoparticles can be followed by FT-IR shown in Fig. 4. It shows a large difference in the bands at 2900 and 1700/cm responsible for oleic acid and oleylamine [20] marked in green on the black for unwashed sample (i). The sample washed with ethanol/hexane (ii) (in blue) still shows presence of organic ligands, while the red spectrum obtained for $LiMnPO_4$ after ligand exchange (iii) shows no more such band. It confirms that oleic acid and oleylamine are successfully removed by the ligand exchange method on the surface of $LiMnPO_4$ nanoparticles.

These finding are confirmed by thermogravimetric analysis (TGA) for the same three samples (see Supplementary data Fig. S2). Unwashed material (i) loses about 15 wt% of the total weight, indicating the amount of remaining surfactants of nanoparticles of $LiMnPO_4$. 10 wt% of the total weight is still lost after washing with ethanol/hexane (ii), indicating that only 1/3 of surfactant can be removed with this method. In contrast, our ligand exchange method leads to only 2 wt% weight loss (iii), proving the efficacy to remove the organic residues after the synthesis. Another strong advantage of this ligand exchange method is to avoid undesired particle growth compared to heating treatments at high temperatures (>500 °C) as used by Doi et al. [24] upon which the nanoparticles aggregate.

3.4. Nanocomposite of C-$LiMnPO_4$

In order to make $LiMnPO_4$ electronically more conductive, carbon black can be added to improve its properties. We have shown previously that addition of carbon black improves the electrochemical properties [13,15]. The typical amount of carbon described in the literature is between 20 and 30 wt% [12,13,15,20].

Among the parameters mentioned in the introduction, we here focus on the lowering of the carbon quantity used to prepare the composite. We chose high surface area of carbon black and the ball milling method to obtain a C-$LiMnPO_4$ nanocomposite with intimate contact between carbon and $LiMnPO_4$. Two nanocomposites are prepared by ball milling, with 5 and 7 wt% of carbon having 1000 m^2/g of specific surface area, respectively, and the $LiMnPO_4$ nanoparticles as obtained in Fig. 1(d), thus with the highest surface area of our prepared nanoparticles (referred to as 5C-$LiMnPO_4$ and 7C-$LiMnPO_4$, respectively). 7C- and 5C-$LiMnPO_4$ nanocomposites are investigated by TEM as shown in Fig. 5(a) and (b), respectively. Carbon is dark gray and $LiMnPO_4$ particles are black in these images. In 7C-$LiMnPO_4$, the carbon seems better distributed and the $LiMnPO_4$ active particles are more homogeneously coated compared to 5C-$LiMnPO_4$, which has more often bare $LiMnPO_4$ particles without carbon coating on the surface (Fig. 5(b)). We also observed that the shape of the $LiMnPO_4$ particles is now polyhederal, which is different from the initial rod shape of pristine $LiMnPO_4$. 7C-$LiMnPO_4$ nanocomposite is also investigated by SEM (Fig. 5(c) and (d)). It shows a rough surface and agglomerated large, dense particles. EDX confirmed that these agglomerated dense particles consist of C, Mn, P and O elements indicating carbon and $LiMnPO_4$ material (Supplementary data Fig. S3).

From the microscopic methods, we concluded that the best nanocomposite is obtained with 7 wt% of carbon by ball milling.

3.5. Electrochemical properties

A typical process of making an electrode includes the use of the C-$LiMnPO_4$, extra carbon and a binder in N-methyl-2-pyrrolidone (NMP). We prepared the electrodes with the nanostructured composite of 7C-$LiMnPO_4$, additional 3 wt% of carbon black and polyvinylidene fluoride (PVDF) as a binder in order to obtain a 10 wt% of carbon in total. The cathode electrode is assembled in a Swagelok type of cell with lithium metal ribbon as a counter electrode and the commercially available lithium ion battery electrolyte.

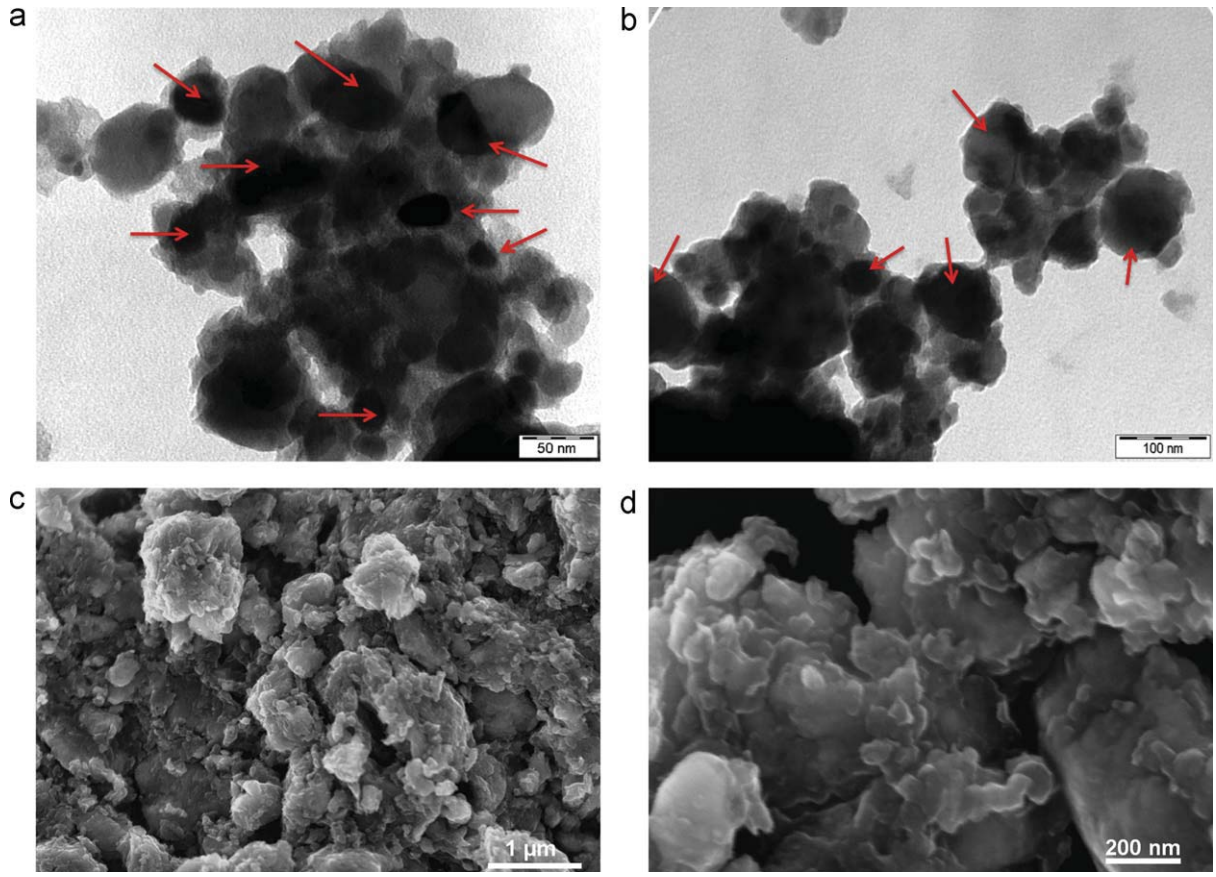

Fig. 5. (a) and (b) TEM images of nanocomposite 7C-$LiMnPO_4$ and 5C-$LiMnPO_4$, respectively. Carbon is dark gray and $LiMnPO_4$ nanoparticles are black, indicated in red arrow. (c) and (d) SEM images of nanocomposite 7C-$LiMnPO_4$. (For interpretation of the references to color in this figure legend, the reader is referred to the web version of the article.)

In Table 2, the literature results for composite C-$LiMnPO_4$ material are resumed for their particle size, amount of carbon added (total amount) and the observed capacity. Compared to these results, Fig. 6 shows that our electrode provided 165 mAh/g of discharge capacity, which is 97% of the theoretical capacity, a value so far unprecedented and obtained at a reasonable C-rate. In the literature, high electrochemical performances of $LiMnPO_4$ electrodes, but lower than ours, are reached only upon adding more than 20 wt% carbon (Table 2) [13,15,20]. However, we improved the electrochemical property by further reducing the particle size below 50 nm of $LiMnPO_4$ using only 10 wt% of carbon in total. This result provides that 10 nm of $LiMnPO_4$ particles can be fully charged and discharged reversibly even with a low quantity of carbon at a reasonable C-rate. This excellent result might be due to the removal of organic material at the surface of the nanoparticles of $LiMnPO_4$.

We also investigated higher C-rates shown in Fig. 7. The discharge capacities of $LiMnPO_4$ electrode are 110 and 66 mAh/g at 1/6 C and 1 C. These capacities of 10 wt% of carbon containing $LiMnPO_4$ nanomaterial are comparable to the ones with ~20 wt% of carbon from other references. The large gap between the charge and the discharge curve at 1 C indicates the resistance of electrode. We currently are optimizing the electrode parameters to reduce its resistance and enhance the performance at high C rates.

Table 2
The comparison of the capacities of $LiMnPO_4$ electrode with various amount of carbon and $LiMnPO_4$ particle size.

Synthesis methods	Particle size (method)	Total C – amount (wt%)	Carbon source	Capacity (mAh/g)	Ref.
Microwave-hydrothermal	100–200 (SEM)	39	Acetylene black	89 at 1/20 C	[18]
Ball milling and thermal heating	240 (laser diffraction)	31.7	Acetylene black	140 at 1/45 C 45 at 1 C	[33]
Liquid phase using oleic acid and oleylamine	7 (TEM) 40–125 (TEM)	25	Acetylene black	6 at 1/100 C 65 at 1/100 C	[24]
Liquid phase using oleic acid and oleylamine	17 (TEM)	25	Acetylene black and carbon nanofiber (VGCF)	153 at 1/100 C 62 at 1/2 C	[20]
Sol-gel	140 (SEM)	20	Acetylene black	134 at 1/10 C 81 at 1 C	[13]
Polyol	30 (TEM)	20	Carbon black	145 at 1/20 C 113 at 1 C	[15]
Ionothermal	300 (SEM)	17.6	Ketjenblack and sucrose	95 at 1/20 C (without CCCV test)	[19]
Hydrothermal	150 × 600 (SEM)	16.8	Acetylene black	126.7 at 1/100 C 113 at 1/10 C	[17]
Ultrasonic spray pyrolysis	10–50 (TEM)	16	Acetylene black	120 at 1/20 C 70 at 1 C	[12]
Liquid phase using oleic acid and oleylamine	10–20 (TEM)	10	Carbon black	165 at 1/40 C 66 at 1 C	This work

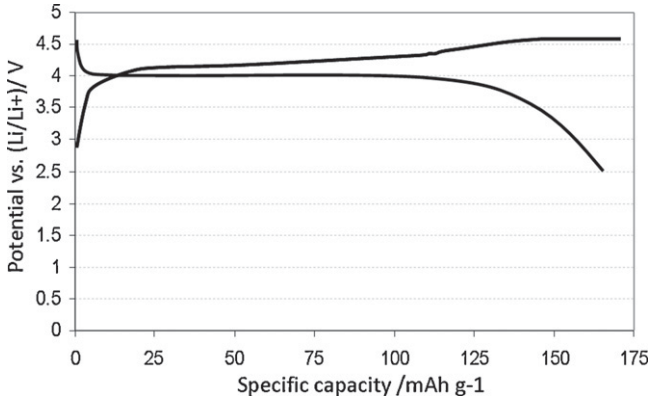

Fig. 6. The charge/discharge curve of $LiMnPO_4$ cathode with 10 wt% of total amount of carbon. It is charged at a constant current rate of 1/40 C to 4.6 V vs. Li and held at 4.6 V vs. Li until 1/100 C, and discharged at a constant current rate of 1/40 C.

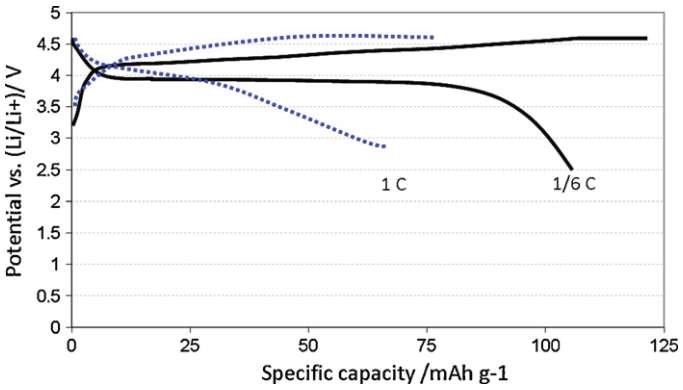

Fig. 7. The charge/discharge curve of $LiMnPO_4$ electrode with 10 wt% of carbon in the voltage window between 2.5 and 4.6 V vs. Li with Li metal as counter electrode and EC:DMC (1:1, v/v) and 1 M $LiPF_6$ electrolyte. It is charged at a constant current rate of 1/6 C (solid line) and 1 C (dot line) to 4.6 V vs. Li and held at 4.6 V vs. Li until 1/50 C, and discharged at a constant current rate of 1/6 C and 1 C.

4. Conclusions

<30 nm of $LiMnPO_4$ nanoparticles are successfully synthesized using thermal decomposition method. The shape and size of $LiMnPO_4$ particles are adjustable using high boiling temperature solvent, tuning the relative concentration of surfactants and the reaction temperature and time. The synthesis using only surfactants without a solvent provides the smallest particle size of 5 nm but low yield of 35%. On the other hand, the synthesis using surfactants and a high boiling point of solvent provides nanorods of 10–20 nm in much higher yield of 78%. In addition, we are able to remove the organic residues efficiently after the synthesis by using a ligand exchange technique without thermal treatment at high temperatures so that we can maintain the initial size of $LiMnPO_4$ nanoparticles.

A nanocomposite of 7 wt% of carbon and $LiMnPO_4$ is provided by ball milling, giving an intimate contact of carbon on $LiMnPO_4$ particles. By adding extra 3 wt% of carbon (total 10 wt% of C) during the electrode processing, we achieved 165 mAh/g (97% of theoretical capacity) at a reasonable C-rate, 1/40 C. To the best of our knowledge, it is the first report obtaining almost full capacity with as little as 10 wt% of carbon additive.

We are currently investigating the influence of the quality of carbon additives on the optimization of cathode preparation, and on the capacities at higher C-rates.

Acknowledgements

This study was supported by the Innovation Fund of the EKZ (Elektrizitätswerke des Kantons Zürich), the Swiss National Science Foundation, FriMat (the Fribourg Center for Nanomaterials) and the University of Fribourg. The authors thank the Celgard and Akzo Nobel for providing the separator and carbon black.

References

[1] J. Cho, Y.J. Kim, T.J. Kim, B. Park, Angew. Chem. Int. Ed. 40 (2001) 3367.
[2] Y.K. Sun, J. Power Sources 83 (1999) 223.
[3] H. Wang, Y.-I. Jang, B. Huang, D.R. Sadowa, Y.M. Chinag, J. Electrochem. Soc. 146 (1999) 473.
[4] Y. Gao, M.V. Yakovleva, W.B. Ebner, Electrochem. Solid-State Lett. 1 (1998) 117.
[5] G.G. Amatucci, J.M. Tarascon, L.C. Klein, Solid State Ionics 83 (1996) 167.
[6] A.K.N. Padhi, K.S. Nanjundaswamy, J.B. Goodenough, J. Electrochem. Soc. 144 (1997) 1188.
[7] A.K. Padhi, K.S. Nanjundaswamy, C. Masquelier, S. Okada, J.B. Goodenough, J. Electrochem. Soc. 144 (1997) 1609.
[8] A. Yamada, S.C. Chung, J. Electrochem. Soc. 148 (2001) A960.
[9] G.H. Li, H. Azuma, M. Tohda, Electrochem. Solid-State Lett. 5 (2002) A135.
[10] M. Yonemura, A. Yamada, Y. Takei, N. Sonoyama, R. Kanno, J. Electrochem. Soc. 151 (2004) A1352.
[11] F. Zhou, K.S. Kang, T. Maxisch, G. Ceder, D. Morgan, Solid State Commun. 132 (2004) 181.
[12] S.-M. Oh, S.-W. Oh, C.-S. Yoon, B. Scrosati, K. Amine, Y.-K. Sun, Adv. Funct. Mater. 20 (2010) 3260.
[13] N.-H. Kwon, T. Drezen, I. Exnar, I. Teerlinck, M. Isono, M. Graetzel, Electrochem, Solid State Lett. 9 (2006) A277.
[14] T. Drezen, N.-H. Kwon, P. Bowen, I. Teerlinck, M. Isono, I. Exnar, J. Power Sources 174 (2007) 949.
[15] D. Wang, H. Buqa, M. Crouzet, G. Deghenghi, T. Drezen, I. Exnar, N.-H. Kwon, J.H. Miners, L. Poletto, M. Grätzel, J. Power Sources 189 (2009) 624.
[16] C. Delacourt, P. Poizot, M. Morcrette, J.M. Tarascon, C. Masquelier, Chem. Mater. 16 (2004) 93.
[17] Y. Wang, Y. Yang, Y. Yang, H. Shao, Solid State Commun. 150 (2010) 81.
[18] H. Ji, G. Yang, H. Ni, S. Roy, J. Pinto, X. Jiang, Electrochim. Acta 56 (2011) 3093.
[19] P. Barpanda, K. Djellab, N. Recham, M. Armand, J.-M. Tarascon, J. Mater. Chem. 21 (2011) 10143.
[20] D. Rangappa, K. Sone, Y. Zhou, T. Kudo, I. Honma, J. Mater. Chem. 21 (2011) 15813–15818.
[21] B. Milke, P. Strauch, M. Antonietti, C. Giordano, Nanoscale 1 (2009) 110.
[22] J.L. Allen, T.R. Jow, J. Wolfenstine, Mater. Res. Soc. Symp. Proc. 1127 (2009), 1127-T1103-1103.
[23] J. Chen, M.J. Vacchio, S. Wang, N. Chernova, P.Y. Zavalij, M.S. Whittingham, Solid State Ionics 178 (2008) 1676.
[24] T. Doi, S. Yatomi, T. Kida, S. Okada, J.-i. Yamaki, Cryst. Growth Des. 9 (2009) 4990.
[25] A.V. Murugan, T. Muraliganth, P.J. Ferreira, A. Manthiram, Inorg. Chem. 48 (2009) 946.
[26] C. Cai, Y. Wang, Materials 2 (2009) 1205.
[27] B. Jin, H.-B. Gu, K.-W. Kim, J. Solid State Electrochem. 12 (2008) 105.
[28] M.M. Doeff, J.D. Wilcox, R. Yu, A. Aumentado, M. Marcinek, R. Kostecki, J. Solid State Electrochem. 12 (2008) 995.
[29] Y. Mizuno, M. Kotobuki, H. Munakata, K. Kanamura, J. Ceram. Soc. Jpn. 117 (2009) 1225.
[30] J. Pyun, Polym. Rev. 47 (2007) 231.
[31] M. Lattuada, T.A. Hatton, Langmuir 23 (2007) 2158.
[32] M. Racuciu, D.E. Creang, A. Airinei, Eur. Phys. J. E 21 (2006) 117.
[33] T. Shiratsuchia, S. Okada, T. Doia, J.-i. Yamaki, Electrochim. Acta 54 (2009) 3145.